

Wind observations of the terrestrial bow shock: 3-D shape and motion

M. Verigin¹, G. Kotova¹, A. Szabo², J. Slavin², T. Gombosi³, K. Kabin⁴, F. Shugaev⁵, and A. Kalinchenko⁵

¹Space Research Institute of Russian Academy of Sciences, Profsoyuznaya, 84/32, Moscow 117810, Russia

²NASA Goddard Space Flight Center, Greenbelt, Maryland 20771, U.S.A.

³University of Michigan, Ann Arbor, MI 48109-2143, U.S.A.

⁴University of Alberta, Edmonton, T6G 2J1, Canada

⁵Moscow State University, Physical Faculty, Moscow 119899, Russia

(Received May 19, 2001; Revised August 2, 2001; Accepted August 13, 2001)

Between late 1994 and early 2001 the Wind orbiter, generally targeted to stay in the solar wind, passed through the Earth's magnetosphere ~ 50 times. About 450 distinct bow shock crossings were collected during the inbound and outbound bracketing each Wind perigee. These crossings and corresponding vectorial upstream solar wind measurements by the Wind MFI and SWE instruments are used to study the 3-D shape of the bow shock and its motion. Mapping of bow shock crossings to the Sun-Earth line and to the terminator plane is realized using a recent analytical model of the planetary bow shock. The asymmetry of the terrestrial bow shock in the terminator plane is studied as a function of Friedrichs diagram anisotropy. Analysis of the subsolar bow shock position as a function of Alfvénic Mach number M_a during intervals of magnetic field aligned solar wind flow shows that the shock tends to approach the Earth when M_a is decreasing, while for non field-aligned flows bow shock moves from the planet.

1. Introduction

Experimental studies of the supersonic solar wind flow past the planets began in 1960s, when the existence of the near-Earth magnetopause and bow shock was reliably established (see e.g., a tutorial review by Russell, 1985). Theoretical investigations began even earlier, in 1959 with the pioneer work of Zhigulev and Romishevsky (1959), which considers the supersonic interaction of conducting fluid with the magnetic field of the Earth. Theoretical modeling of the near planetary bow shocks generally use hydrodynamic, magnetohydrodynamic or semikinetic approaches (e.g., Spreiter *et al.*, 1966; Cairns and Lyon, 1995; Tanaka, 1995; Brecht, 1997; Kabin *et al.*, 2000). These models, especially of latter two kinds, need plenty of processor time for even a single run on modern supercomputers, and that is why they cannot be used for the routine analysis of the bow shock position and shape when the external solar wind parameters continuously change.

Analysis of a lot of collected experimental data relevant to the bow shock observations requires a convenient analytical model, and generally empirical models are used (Fairfield, 1971; Formisano, 1979; Slavin and Holzer, 1981). A review of pertinent studies is given in the paper by Peredo *et al.* (1995) presenting the latest empirical model of the terrestrial bow shock. Though providing general description of the average shape and position of the bow shock, empirical models have uncertain limits of applicability and fail for unusual solar wind conditions. Besides, in these models the bow shock shape is usually described by a conic section, has

incorrect asymptotic behavior unless distant crossings are included (Slavin *et al.*, 1984), and do not consider specific heat ratio influence on the planetary bow shock position.

In the present paper a recently developed semi-empirical bow shock model (Verigin *et al.*, 1997, 1999) is used for the analysis of the terrestrial bow shock crossings recorded by the Wind spacecraft. Similar analysis of the bow shock asymmetries and behavior was performed using the Interball/Magion 4 data (Verigin *et al.*, 2000). The bow shock modeling approach is based on simultaneous use of analytical MHD formulas and empirical relations describing bow shock characteristics as functions of external solar wind parameters. The Wind experimental data are specially normalized to take into account both variations of the magnetopause stand off distance and curvature due to changes of the solar wind ram pressure and magnetic field. The results of the analysis are given below after presenting the overview of the data, a brief description of the model and the data analysis techniques.

2. Experimental Data

In this study the terrestrial bow shock position and shape are analyzed using experimental data collected by the Wind spacecraft. This spacecraft was primarily maintained in the solar wind but it crosses the bow shock over a wide range of distance. The data set includes 462 bow shock crossings observed since the commissioning of the instruments in late 1994 to the beginning of 2001. Interplanetary magnetic field measurements were provided by the Magnetic Field Investigation experiment (MFI, Lepping *et al.*, 1995) and plasma parameters were taken from the Solar Wind Experiment (SWE, Ogilvie *et al.*, 1995). Magnetic field data were first averaged over the time intervals of plasma mea-

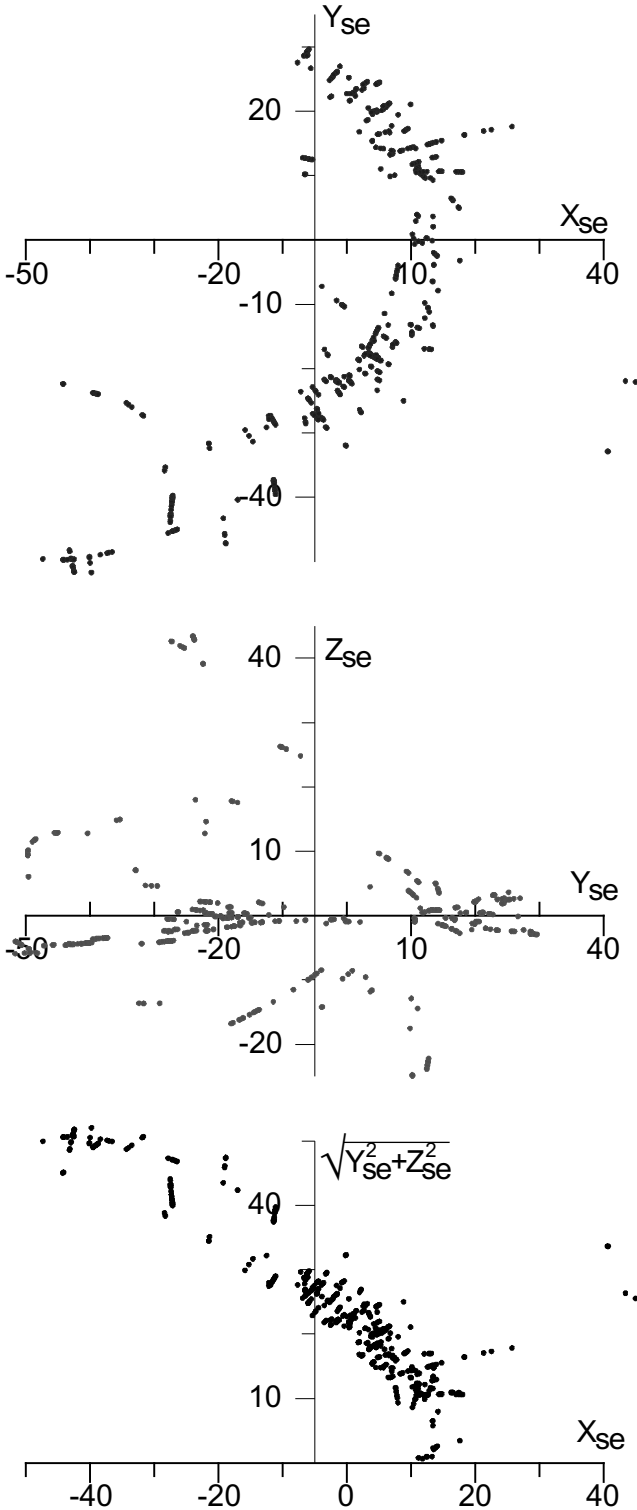


Fig. 1. Distribution of bow shock crossings observed by the Wind spacecraft.

surement (~ 92 s) and then the data obtained just upstream of the bow shock were chosen for our analysis as a proxy for the undisturbed solar wind parameters (neglecting, e.g., their modification due to possible foreshock presence).

Figure 1 presents all of the Wind bow shock crossings in the (X_{se}, Y_{se}) and (Y_{se}, Z_{se}) planes of the geocentric solar ecliptic reference frame and in cylindrical coordinates

$(X_{se}, \sqrt{Y_{se}^2 + Z_{se}^2})$. The crossings are spread from the subsolar region down to $X_{se} \approx -50 R_e$ with most crossings occurring at low latitudes, i.e. $|Z_{se}| < 10 R_e$.

3. Bow Shock Model

The most convenient reference frame for the bow shock description is the geocentric interplanetary medium GIPM frame, where X_{gipm} is antiparallel to the upstream solar wind velocity vector and IMF field line lies in the second–fourth quadrant of the (X_{gipm}, Y_{gipm}) plane (Peredo *et al.*, 1995). Use of this reference frame implies symmetry of the magnetopause that is generally invalid, e.g., due to the presence of the cusp regions. But this assumption seems to be reasonably valid for the subsolar part of the magnetopause mostly influencing the bow shock position and shape because of subsonic flow in the adjacent magnetosheath.

The bow shock standoff distance Δ and the curvature radius of its nose R_s can be deduced from the following relations (Verigin *et al.*, 1997, 1999):

$$\begin{aligned} \Delta &= R_0 b^{-2/5} (b\epsilon' / (1.87 + 0.86/(b\epsilon')^{3/5}))^{2/3}, \\ R_s &= R_0 b^{-3/4} ((1.058 + b\epsilon') / 1.067)^{5/3}, \end{aligned} \quad (1)$$

where R_0 is the nose curvature radius of the magnetopause, $\epsilon' = \epsilon / (1 - \epsilon)$ is the reduced compression of the solar wind flow, and $\epsilon = \rho_1 / \rho_2$ is the ratio of the solar wind densities upstream ρ_1 and downstream ρ_2 of the bow shock nose. In MHD calculations ϵ appears as the real root of a cubic equation directly deduced from Rankine-Hugoniot relations (e.g., Zhuang and Russell, 1981):

$$\begin{aligned} \epsilon^3 - \left(\frac{\gamma - 1}{\gamma + 1} + \frac{\gamma + (\gamma + 2) \cos^2 \vartheta_{bv}}{(\gamma + 1) M_a^2} + \frac{2}{(\gamma + 1) M_s^2} \right) \epsilon^2 \\ - \frac{\cos^2 \vartheta_{bv}}{(\gamma + 1) M_a^4} \left(\gamma - 1 + \frac{2 \cos^2 \vartheta_{bv}}{M_s^2} \right) \\ + \frac{1}{(\gamma + 1) M_a^2} \left(\gamma (1 + \cos^2 \vartheta_{bv}) - 2 \right. \\ \left. + \cos^2 \vartheta_{bv} \left(\frac{\gamma + 1}{M_a^2} + \frac{4}{M_s^2} \right) \right) \epsilon = 0, \end{aligned} \quad (2)$$

where M_a , M_s are the upstream Alvenic and sonic Mach numbers, respectively, and ϑ_{bv} is the angle between the solar wind velocity and interplanetary magnetic field vectors.

It was shown by Verigin *et al.* (1997, 1999) that relations (1) with a factor $b = 1$ agrees well with the results of HD calculations by Spreiter and Stahara (1995) and have the correct asymptotic behavior when $M_s, \epsilon \rightarrow 1$. Taking into account the MHD Rankine-Hugoniot relation for the curved shock we have introduced the factor $b = 1 - \cos^2 \vartheta_{bv} / \epsilon M_a^2$ that permits us to reproduce the results of Spreiter and Rizzi (1974) including the approaching of the bow shock to the obstacle with decreasing Alvenic Mach number for field-aligned MHD flow.

Unusual, from the first glance, approaching of the bow shock to the obstacle has quite simple physical explanation. Really, the ability of the usual HD flow to divert its direction is determined by the ratio of the disturbance propagation velocity in the direction perpendicular to the flow (sonic velocity V_s), to the flow velocity V itself. Large increase of V_s and

decrease of V after a strong shock with $\varepsilon \rightarrow (\gamma - 1)/(\gamma + 1)$ provide great ability for flow diversion around the obstacle and thus lead to small equilibrium standoff distance Δ in this case. Smaller value of V_s/V after a weak shock leads to lower ability for diversion of the flow and to larger Δ . As follows from Eq. (2) introduction of the flow-aligned magnetic field ($\vartheta_{bv} = 0$) will not change the strength of the shock (the value of ε) in the stagnation line vicinity because the HD value of $\varepsilon = ((\gamma - 1)M_s^2 + 2)/(\gamma + 1)/M_s^2$ remains to be the root of this equation for any M_a . However in this case the disturbance propagation velocity in the direction perpendicular to the flow is magnetosonic V_{ms} (but not sonic). The higher value of V_{ms}/V in the field aligned MHD flow (compared to smaller V_s/V value in HD flow) provides better ability for diversion of the flow around the obstacle and thus smaller equilibrium standoff distance Δ .

The equation for a quasi-hyperbolic bow shock surface with the standoff distance Δ and nose curvature radius R_s defined above, can then be written in the following form as shown by Verigin *et al.* (1999):

$$X_{gipm} = r_0 + \Delta + \chi R_s (M_{as}^2 - 1) - \frac{1}{2}(1 - \chi) \sqrt{(M_{as}^2 - 1) \cdot (Y_{gipm}^2 + Z_{gipm}^2)} - \chi R_s (M_{as}^2 - 1) \cdot \sqrt{1 - \frac{(1 - \chi)}{\chi R_s} \sqrt{\frac{Y_{gipm}^2 + Z_{gipm}^2}{M_{as}^2 - 1}} + \frac{(1 + \chi)^2 \cdot (Y_{gipm}^2 + Z_{gipm}^2)}{4\chi^2 R_s^2 (M_{as}^2 - 1)}}} \quad (3)$$

where r_0 is a geocentric distance to the magnetopause nose, $M_{as} = 1/\sin \vartheta_{as}$ is a function of the asymptotic downstream slope ϑ_{as} of the bow shock (Mach cone), and a shaping parameter $\chi = 3.2/(M_{as} + 1)$. (N.B., equation (10) in Verigin *et al.* (1997) was published with misprints, and the updated relation for χ is given here.) The ϑ_{as} (and M_{as}) parameters may be determined geometrically using the Friedrichs diagram for fast MHD waves, e.g., see figure 4 of Spreiter *et al.* (1966). For the sake of completeness we note that M_{as} can also be determined from:

$$M_{as}^2 \left(M_a^2 + M_s^2 - \left(\cos \vartheta_{bv} - Y_{gipm} \sin \vartheta_{bv} \sqrt{(M_{as}^2 - 1)/(Y_{gipm}^2 + Z_{gipm}^2)} \right)^2 \right) = M_a^2 M_s^2. \quad (4)$$

For the determination of magnetopause nose curvature radius, R_0 , and geocentric distance to its nose r_0 we used the model of the magnetopause size and shape introduced by Shue *et al.* (1997, 1998). In this model geocentric distance to the magnetopause r is a function of the angular distance ϑ from the X_{gipm} axis: $r = r_0(2/(1 + \cos \vartheta))^\alpha$ with

$$r_0 = r_0(\rho V^2, B_z) = (10.22 + 1.29 \tanh(0.184(B_z + 8.14))) \cdot (\rho V^2)^{-1/6.6} \quad \text{and} \quad (5) \\ \alpha = \alpha(\rho V^2, B_z) = (0.58 - 0.07B_z) \cdot (1 + 0.024 \ln(\rho V^2))$$

Both magnetopause parameters are functions of the solar wind ram pressure $-\rho V^2$ [nPa] and the B_z [nT] component

of the interplanetary magnetic field (Shue *et al.*, 1998). The nose curvature radius R_0 of the magnetopause is derived as:

$$R_0 = R_0(\rho V^2, B_z) = 2r_0(\rho V^2, B_z)/(2 - \alpha(\rho V^2, B_z)). \quad (6)$$

4. Data Analysis Technique

Figure 2 presents two examples, December 22–23, 1995 and May 5–6, 1999, of plasma parameter variations (magnetic field magnitude (a), Mach numbers (c), and ram pressure (d)) and radial distance to the spacecraft and to the modeled bow shock along the same direction (b). Well correspondence is seen between the observed and modeled positions of the spacecraft in both cases. Note that interplanetary shock was crossed at 15.40 on May 5 that resulted in bow shock moving towards the Earth from the spacecraft and thus it was passed by the spacecraft only ~ 4 hours later.

In Fig. 3 the observed distances from the center of the Earth to the point of bow shock crossing r_{obs} are compared with calculated distances to the model bow shock in the direction of real crossing r_{mod} . In this figure the bow shock crossings marked by crosses correspond to ‘outbound’ crossings when Wind turned to be in the solar wind after crossing of the boundary. For ‘inbound’ crossings (dots in Fig. 3) Wind pass to the magnetosheath after bow shock crossing. Solid line in Fig. 3 $r_{mod} = k_{in} r_{obs} = (1.01 \pm 0.02) \cdot r_{obs}$ is the best fitting one for the inbound crossings while the dashed line in this figure $r_{mod} = k_{out} r_{obs} = (0.97 \pm 0.02) \cdot r_{obs}$ is the best fit for the outbound crossings ($\pm 3\sigma$ errors are given). Rather good coincidence of the observed and modeled distances $r_{mod} \approx r_{obs}$ justifies the use of the model described by relations (1–6) for the analysis of the data.

On the other hand, we may interpret a small difference between the coefficients 0.97 obtained for the outbound crossings and 1.01 for inbound crossings as a consequence of motion of the bow shock, which, generally speaking, never reaches its equilibrium position due to solar wind temporal variations. For the geocentric distances where Wind observed the bow shock crossings, we expect that the orbital velocity of the spacecraft is usually much less than possible velocity of the bow shock itself (sonic, Alfvénic, fraction of the solar wind velocity). In other words, it is not the spacecraft that crosses the standing bow shock, but the bow shock moves past the nearly standing spacecraft on the way to new ‘equilibrium’ positions. Hence the equilibrium model bow shock, calculated with the use of solar wind parameters measured after the outbound crossing, should be closer to the planet than the observed bow shock position $k_{out} < 1$, and vice versa the equilibrium model bow shock, calculated with the use of solar wind parameters measured before the inbound crossing, should be further from the planet than the observed bow shock position $k_{in} > 1$.

For the analysis of bow shock behavior in the subsolar region and in the terminator plane it is necessary to ‘project’ the observed points of bow shock crossings to these regions. Every crossing point r_{obs} was projected to $X_{gipm}(r_p^0)$ and to GIPM ‘terminator’ plane (r_p^{90}) along the modeled bow shock surface (dashed line in Fig. 4) in the plane containing the X_{gipm} axis and this point: $r_p^0 = r_{obs} \cdot r_{mod}^0/r_{mod}$ and $r_p^{90} = r_{obs} \cdot r_{mod}^{90}/r_{mod}$, where r_{mod} , r_{mod}^0 , r_{mod}^{90} are the dis-

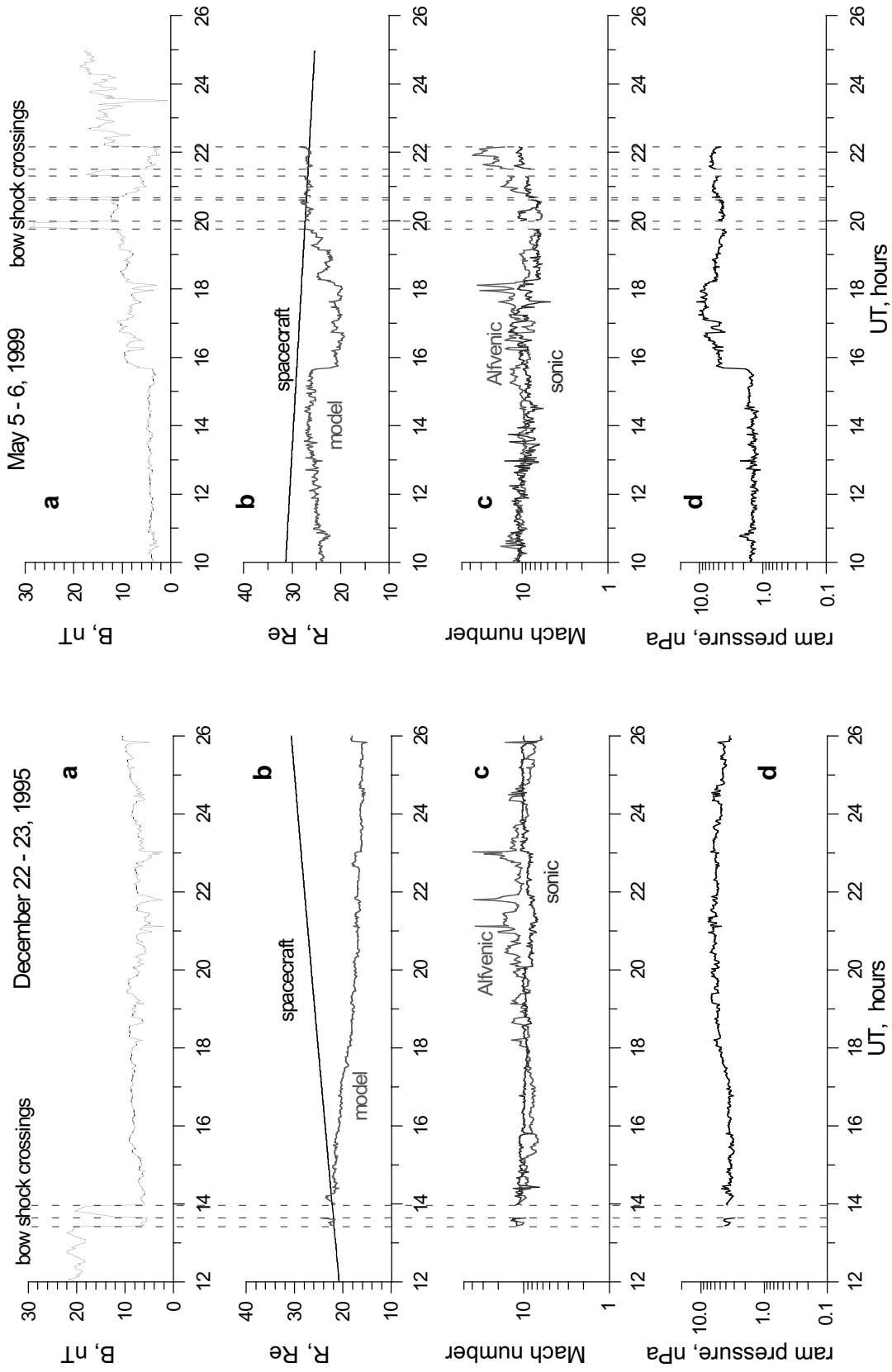


Fig. 2. Variations of the magnetic field magnitude (a), Mach numbers (c) and ram pressure (d), and radial distance to the spacecraft and to the modeled bow shock (b) along the Wind spacecraft trajectory in its outbound pass on December 22–23, 1995 (left panels) and inbound pass on May 5–6, 1999 (right panels).

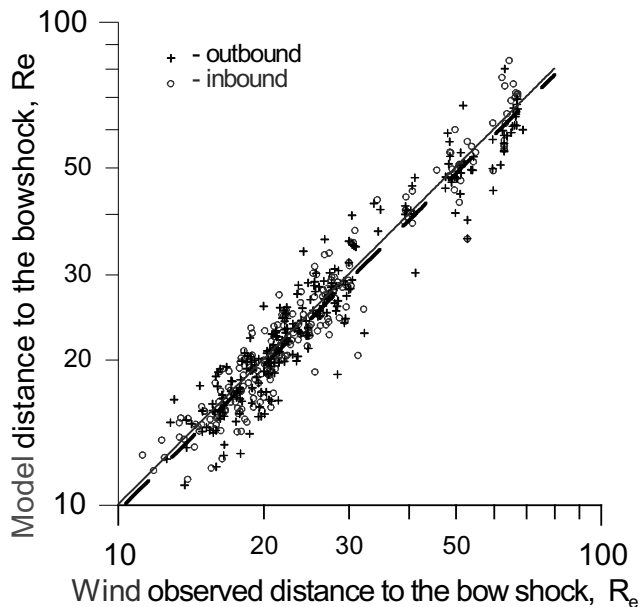


Fig. 3. Scatter plot of the observed and modeled distances to the bow shock.

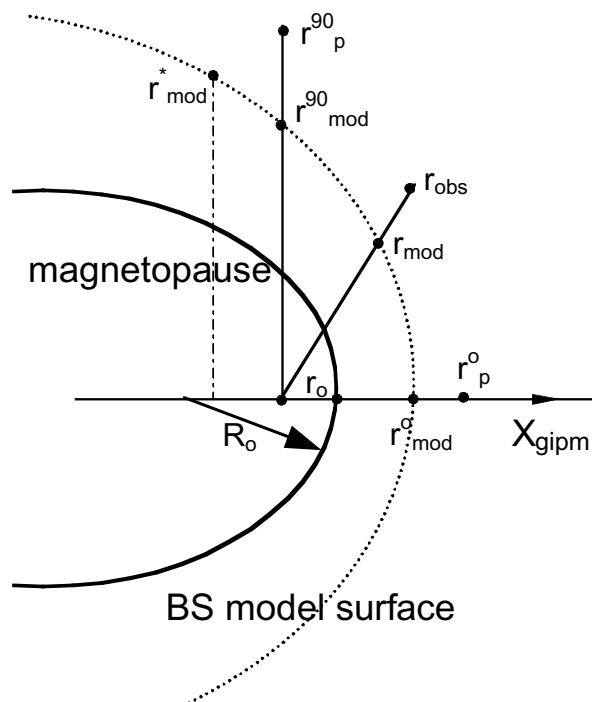


Fig. 4. Illustration of projection of the observed points of bow shock crossings to the terminator plane and to the X_{gipm} axis.

tances to the modeled shock surface in the direction of the observed crossing, in the X_{gipm} direction, and in perpendicular to X_{gipm} direction, respectively (Fig. 4).

Then the projected bow shock crossings must be normalized to ‘standard’ solar wind conditions $-V^2 = 1$ nPa and $B_z = 0$ nT. Let r_n be the geocentric distance to the magnetopause nose and R_n be its (7) curvature radius calculated by relations (5, 6) under the standard solar wind conditions:

$r_n = r_o(1 \text{ nPa}, 0 \text{ nT})$, $R_n = R_o(1 \text{ nPa}, 0 \text{ nT})$. Uniform scaling of the space by a factor R_n/R_o and subsequent shift along the X_{gipm} axis by a value $(r_n - r_o \cdot R_n/R_o)$ will transform both modeled magnetopause nose curvature radius R_o and its nose position r_o (Fig. 4) into R_n and r_n . Simultaneously

$$r_p^0 \rightarrow r_{pn}^0 = r_p^0 R_n/R_o + (r_n - r_o R_n/R_o),$$

thus providing possibility to find r_{pn}^0 —the observed magnetopause crossing position projected to X_{gipm} and normalized.

In order to find normalized position of observed magnetopause crossing projected to (8) normalized GIPM ‘terminator’ plane r_{pn}^{90} we should first determine r_{mod}^* —the distance to the modeled magnetopause from the point with $X_{\text{gipm}} = -(r_n R_o/R_n - r_o)$ and $Y_{\text{gipm}} = 0$ in the direction perpendicular to X_{gipm} axis in the plane containing this axis and observed location of the bow shock (Fig. 4). Then scaling by the factor R_n/R_o will move r_{mod}^* to the r_{pn}^{90} :

$$r_{pn}^{90} = r_{\text{mod}}^* R_n/R_o.$$

It is expected that, after the normalization of projected bow shock positions (Eq. (7), (8)), the position of normalized bow shock will be a function of only M_a , M_s Mach numbers and ϑ_{bv} .

5. Results

Figure 5(a) presents a scatter plot of the bow shock crossings recorded by Wind and projected to the X_{gipm} axis (r_p^0 —see Fig. 4) as a function of the solar wind ram pressure. Large scattering of experimental data in this traditional presentation permits their approximation by different functional dependencies, including simple power relation $r_p^0 \sim (-V^2)^{-1/6}$ (dashed line in Fig. 5(a)), which follows from oversimplified assumption on self-similar simultaneous motions of the bow shock and magnetopause. The same data set but normalized by relation (7) demonstrates expected independence on $-V^2$ of normalized bow shock crossings $r_{pn}^0 \sim \text{const}$ (dashed line in Fig. 5(b)) thus confirming the reasonability of the used normalization approach, though again with a large scatter.

Both in Figs. 5(a), (b) bow shock crossings occurring during intervals of very low solar wind ram pressure (e.g., April 27; May 11, 1999; May 2, 2000) lie clearly out of dashed lines and this is likely caused by strong dependence of the bow shock position on M_a in this case (see Fairfield *et al.*, 2001). In order to study dependence of the bow shock position on M_a , M_s , and ϑ_{bv} let us sort normalized and projected crossings into different boxes according to these parameters.

Bow shock (r_{pn}^0) behavior as a function of Alfvénic Mach number for rather high values of sonic Mach number ($M_s > 7.5$) in different ranges of ϑ_{bv} is analyzed in Fig. 6. Smooth curves in this figure are the same functional dependencies $r_{pn}^0 = 14.5 R_e + \text{const}/\sqrt{M_a^2 - 1}$ with const fitting the data. For quasi-perpendicular and inclined solar wind flows a familiar motion of the subsolar bow shock from the obstacle with the decrease of Mach number M_a is observed. The subsolar bow shock rapidly gets away from the planet for quasi-perpendicular flow (top panel) and slower moves away for inclined flow (middle panel). For quasi-parallel solar wind

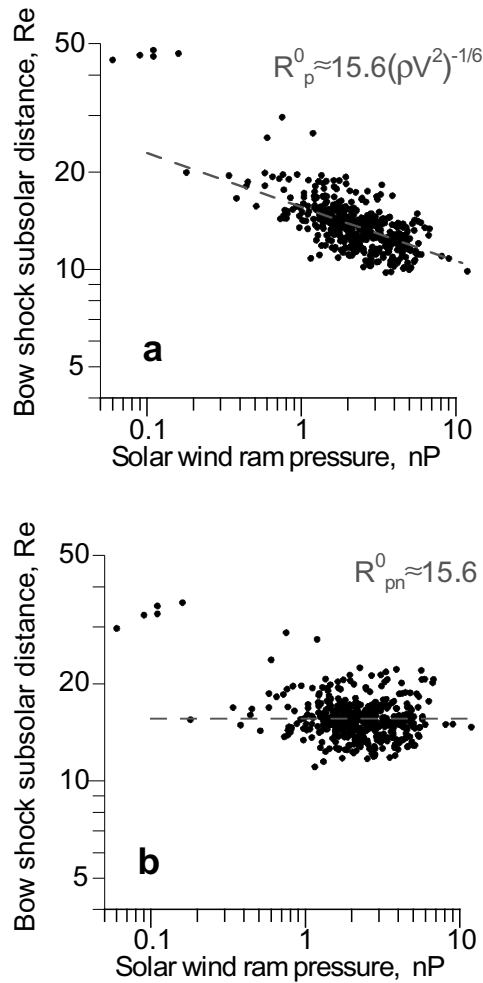


Fig. 5. Locations of bow shock crossings mapped to X_{se} as a function of solar wind ram pressure: unnormalized (a) and normalized (b).

flow the bow shock tends to move towards the Earth with M_a decreasing (bottom panel). This last fact supplements the result obtained by the Magion 4/Interball 1 data (Verigin *et al.*, 2000, 2001).

In none of the previous analysis of observational data this effect was found, though it was predicted by theoretical models (Spreiter and Rizzi, 1974; Cairns and Lyon, 1995). Empirical model of Peredo *et al.* (1995) shows that the subsolar shock moves earthward while the flanks move outward in response to decreasing M_a , but the authors did not divide the cases according to ϑ_{bv} and this seems to be important (cf. top and bottom panels in Fig. 6). Another study by Slavin *et al.* (1996) found that the bow shock was everywhere closer to the magnetopause when the interplanetary magnetic field is nearly aligned with the solar wind flow direction.

The bow shock shape asymmetry found in the terminator plane is illustrated in Fig. 7, where normalized projections of bow shock crossings (r_{pn}^{90}) are shown in polar coordinates as a function of the clock angle φ : $\varphi = 0^\circ$ corresponds to $+Y_{gipm}$ and $\varphi = 90^\circ$ —to $+Z_{gipm}$ directions. In order to decrease the scattering effect due to large range of subsolar bow shock distances, only the cases with ram pressure normalized subsolar distances in the interval $12 R_e < r_{pn}^0 < 16 R_e$ are considered. Then the data are binned by ϑ_{bv} , and

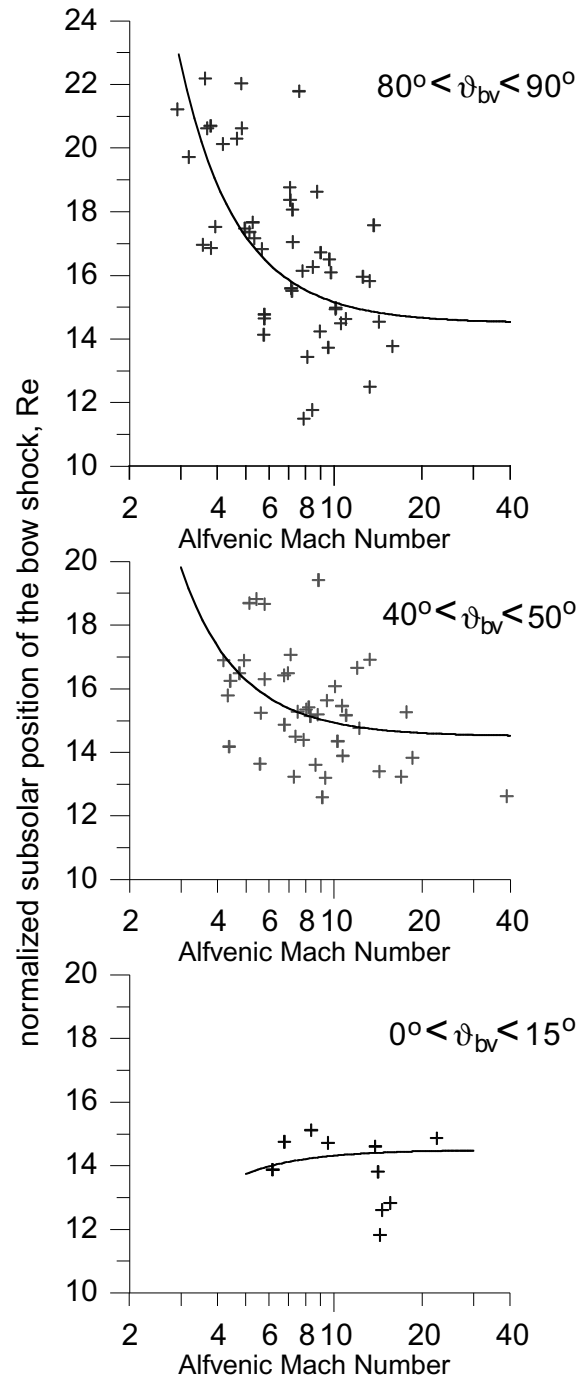


Fig. 6. Dependence of V^2 normalized subsolar position of the bow shock on Alfvénic Mach number. $M_s > 7.5$.

subdivided into 2 cases with low and high anisotropy of Friedrichs diagram, since far from the planet bow shock anisotropy is expected to be influenced by the anisotropy of fast magnetosonic wave propagation. From Fig. 7 it is seen that the cross section of the bow shock in the terminator plane is almost symmetric in the cases with low anisotropy of phase velocity of fast magnetosonic wave. (The $\pm Y_{gipm}$, $\pm Z_{gipm}$ semi-axes and the shifts of the center δY_{gipm} of approximating ellipses are gathered in Table 1 for all bins). For highly anisotropic field-aligned flows the bow shock is still symmetric, while quasi-perpendicular flows with highly

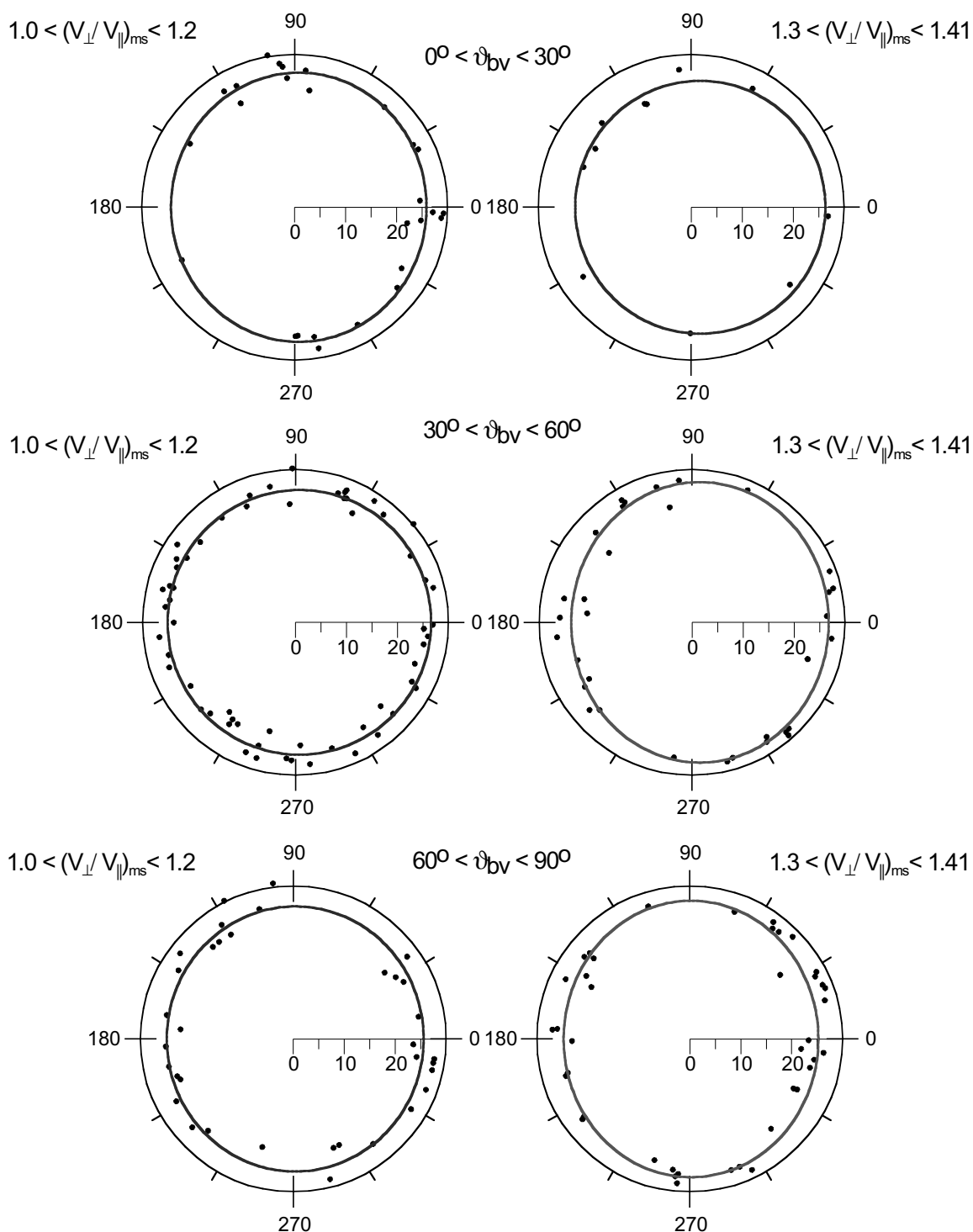


Fig. 7. Projections of normalized bow shock crossings to the terminator plane for quasi-field aligned, inclined, and quasi-perpendicular solar wind flows, subdivided into cases with low and high anisotropy of phase velocity of fast magnetosonic wave. $12 R_e < r_{pn}^0 < 16 R_e$.

anisotropic Friedrichs diagram result in bow shock elongated in $\pm Z_{\text{gipm}}$ direction at the terminator. In the case of inclined anisotropic flows the terminator bow shock cross section is elongated in the $\pm Z_{\text{gipm}}$ direction (ratio of the axes ~ 1.1) and shifted toward positive Y_{gipm} values by $\delta Y_{\text{gipm}} \sim 1.5 R_e$. This analysis of the bow shock asymmetry is again in agreement with the preliminary study based on Magion 4/Interball 1 data, but there only inclined flow was consid-

ered. A similar, but weaker effect was found by Peredo *et al.* (1995) without distinguishing the cases of isotropic and non-isotropic Friedrichs diagram. The Earth's bow shock model constructed by Bennett *et al.* (1997) also exhibits qualitatively similar elongation and shift of the bow shock cross section but far downstream from the planet at $X_{\text{gipm}} \approx -100 + -350 R_e$.

Table 1. Semi-axes and shifts of the centers of best fit ellipses approximating terminator cross-section of the terrestrial bow shock.

		$1.0 < (V_{\perp}/V_{\parallel})_{ms} < 1.2$	$1.3 < (V_{\perp}/V_{\parallel})_{ms} < 1.41$
$0^{\circ} < \vartheta_{bv} < 30^{\circ}$	$\pm Y_{gipm}$	25.1	(24.6)
	$\pm Z_{gipm}$	26.4	(24.8)
	δY_{gipm}	0.8	(1.7)
$30^{\circ} < \vartheta_{bv} < 60^{\circ}$	$\pm Y_{gipm}$	25.9	25.3
	$\pm Z_{gipm}$	26.0	27.5
	δY_{gipm}	0.7	1.5
$60^{\circ} < \vartheta_{bv} < 90^{\circ}$	$\pm Y_{gipm}$	25.2	25.0
	$\pm Z_{gipm}$	26.0	27.1
	δY_{gipm}	0.4	0.2

6. Conclusions

About 450 distinct bow shock crossings observed in inbound and outbound legs of the Wind spacecraft trajectory and corresponding vectorial upstream solar wind measurements by Wind SWE and MFI instruments are used to study the 3-D shape and motion of the terrestrial bow shock. Mapping of bow shock crossings to the Sun-Earth line and to the terminator plane is realized using a recently developed semi-empirical model of the planetary bow shock. The data analysis technique includes a new way of bow shock normalization that fixes both the magnetopause nose position and curvature radius.

Rather good coincidence of the observed and modeled distances to the bow shock $r_{\text{mod}} \approx r_{\text{obs}}$ justifies the applicability of the model used. On the other hand, positions of the inbound crossings slightly closer to the planet in comparison to the modeled ones, and correspondingly, slightly further positions of the outbound crossings result from the non steady nature of the boundary.

Analysis of the subsolar bow shock position as a function of Alfvénic Mach number shows that for field-aligned flows of the solar wind, the shock tends to approach the Earth when M_a is decreasing, while for non field-aligned flows the bow shock moves from the planet.

The asymmetry of the terrestrial bow shock shape in the terminator plane is studied as a function of Friedrichs diagram anisotropy. Inclined solar wind flows with high anisotropy of phase velocity of fast magnetosonic wave result in the formation of the bow shock with terminator cross section elongated in north-south GIPM direction and shifted toward positive Y_{gipm} values.

Acknowledgments. Discussions with D. H. Fairfield are gratefully acknowledged. This work was performed while one of the authors (MV) held a NRC Associateship Award at NASA/GSFC.

References

Bennett, L., M. G. Kivelson, K. K. Khurana, L. A. Frank, and W. R. Paterson, A model of the Earth's distant bow shock, *J. Geophys. Res.*, **102**(A12), 26927–26941, 1997.
 Brecht, S. H., Hybrid simulation of the magnetic topology of Mars, *J. Geophys. Res.*, **102**, 4743–4750, 1997.
 Cairns, L. H. and J. G. Lyon, MHD simulations of the Earth's bow shock at low Mach numbers: Stand-off distances, *J. Geophys. Res.*, **100**, 17173, 1995.

Fairfield, D. H., Average and unusual locations of the Earth's magnetopause and bow shock, *J. Geophys. Res.*, **76**, 6700, 1971.
 Fairfield, D. H., I. H. Cairns, M. D. Desch, A. Szabo, A. J. Lazarus, and M. R. Aellig, The location of low Mach number bow shocks at Earth, *J. Geophys. Res.*, **106**, 2001 (accepted).
 Formisano, V., Orientation and shape of the Earth's bow shock in three dimensions, *Planet. Space Sci.*, **27**, 1151, 1979.
 Kabin, K., T. I. Gombosi, D. L. DeZeeuw, and K. G. Powell, Interaction of Mercury with the solar wind, *Icarus*, **143**, 397–406, 2000.
 Lepping, R. P., M. Acuna, L. Burlaga, W. Farrell, J. Slavin, K. Schatten, F. Mariani, N. Ness, F. Neubauer, Y. C. Whang, J. Byrnes, R. Kennon, P. Panetta, J. Scheifele, and E. Worley, The Wind magnetic field investigation, *Space Sci. Rev.*, **71**, 207–229, 1995.
 Ogilvie, K. W., D. J. Chorney, R. J. Fitzenreiter, F. Hunsaker, J. Keller, J. Lobell, G. Miller, J. D. Scudder, E. C. Sittler, Jr., R. B. Torbert, D. Bodet, G. Needell, A. J. Lazarus, J. T. Steinberg, J. H. Tappan, A. Mavretic, and E. Gergin, SWE a comprehensive plasma instrument for the Wind spacecraft, *Space Sci. Rev.*, **71**, 55–77, 1995.
 Peredo, M., J. A. Slavin, E. Mazur, and S. A. Curtis, Three-dimensional position and shape of the bow shock and their variation with Alfvénic, sonic and magnetosonic Mach numbers and interplanetary magnetic field orientation, *J. Geophys. Res.*, **100**, 7907–7916, 1995.
 Russell, C. T., Planetary bow shocks, in *Collisionless Shocks in the Heliosphere: A Tutorial Review*, Geophys. Monogr. Ser., vol. 35, edited by B. T. Tsurutani and R. G. Stone, AGU, Washington, D.C., pp. 109–130, 1985.
 Shue, J.-H., J. K. Chao, H. C. Fu, C. T. Russell, P. Song, K. K. Khurana, and H. J. Singer, A new functional form to study the solar wind control of the magnetopause size and shape, *J. Geophys. Res.*, **102**(A5), 9497–9511, 1997.
 Shue, J.-H., P. Song, C. T. Russell, J. T. Steinberg, J. K. Chao, G. Zastenker, O. L. Vaisberg, S. Kokubun, H. J. Singer, T. R. Detman, and H. Kawano, Magnetopause location under extreme solar wind conditions, *J. Geophys. Res.*, **103**(A8), 17691–17700, 1998.
 Slavin, J. A. and R. E. Holzer, Solar wind flow about the terrestrial planets, 1. Modelling bow shock position and shape, *J. Geophys. Res.*, **86**, 11401, 1981.
 Slavin, J. A., R. E. Holzer, J. R. Spreiter, and S. S. Stahara, Planetary Mach cones: Theory and observation, *J. Geophys. Res.*, **89**(A5), 2708–2714, 1984.
 Slavin, J. A., A. Szabo, M. Peredo, C. J. Owen, R. P. Lepping, R. Fitzenreiter, R. W. Ogilvie, J. L. Stremberg, and A. J. Lazarus, Near-simultaneous bow shock crossings by wind and IMP 8 on December 1, 1994, *Geophys. Res. Lett.*, **23**(1), 207, 1996.
 Spreiter, J. R. and A. W. Rizzi, Aligned magnetohydrodynamic solution for solar wind flow past the Earth's magnetosphere, *Acta Astronaut.*, **1**, 15–55, 1974.
 Spreiter, J. R. and S. S. Stahara, The location of the planetary bow shocks: A critical overview of theory and observations, *Adv. Space Res.*, **15**(8/9), 433, 1995.
 Spreiter, J. R., A. L. Summers, and A. Y. Alksne, Hydromagnetic flow around the magnetosphere, *Planet. Space Sci.*, **14**, 223, 1966.
 Tanaka, T., Generation mechanism for magnetosphere-ionosphere current system deduced from a three-dimensional MHD simulation of the solar

- wind-magnetosphere-ionosphere coupling processes, *J. Geophys. Res.*, **100**(A7), 12057–12074, 1995.
- Verigin, M. I., G. A. Kotova, A. P. Remizov, N. M. Shutte, K. Schwingenschuh, W. Riedler, M. Delva, H. Rosenbauer, K. Szego, M. Tatrallyay, and V. Styazhkin, Studies of the Martian bow shock response to the variation of the magnetosphere dimensions according to TAUS and MAGMA measurements aboard the PHOBOS 2 orbiter, *Adv. Space Res.*, **20**(2), 155–158, 1997.
- Verigin, M. I., G. A. Kotova, A. P. Remizov, V. A. Styazhkin, N. M. Shutte, T.-L. Zhang, W. Riedler, H. Rosenbauer, K. Szego, M. Tatrallyay, and K. Schwingenschuh, Shape and location of planetary bow shocks, *Cosmic Research*, **37**(1), 34–39, 1999.
- Verigin, M., G. Kotova, A. Remizov, V. Bezrukikh, O. Plokhova, J. Slavin, A. Szabo, M. Kessel, J. Safrankova, Z. Nemecek, T. Gombosi, K. Kabin, F. Shugaev, and A. Kalinchenko, in *Proceedings of International Symposium "From solar corona through interplanetary space, into Earth's magnetosphere and ionosphere: Interball, ISTP satellites, and ground-based observations"*, February 1–4, 2000, Kyiv, Ukraine, pp. 289–293.
- Verigin, M. I., G. A. Kotova, J. Slavin, A. Szabo, M. Kessel, J. Safrankova, Z. Nemecek, T. I. Gombosi, K. Kabin, F. Shugaev, and A. Kalinchenko, Analysis of the 3-D shape of the terrestrial bow shock by Interball/Magion 4 observations, in *33rd COSPAR Scientific Assembly, 16-23 July 2000*, Warsaw, Poland, Program Book, Warsaw, 2000, p. 106, 136 (*Adv. Space Res.*, 2001, accepted).
- Zhigulev, V. N. and E. A. Romishevsky, Concerning the interaction of currents flowing in a conducting medium with the Earth's magnetic field, *Doklady Akad. Nauk SSSR*, **127**, 1001–1004, 1959 (in Russian), (English translation: *Soviet Phys. Doklady*, **4**, 859–862, 1960).
- Zhuang, H. C. and C. T. Russell, An analytic treatment of the structure of the bow shock and magnetosheath, *J. Geophys. Res.*, **86**, 2191–2205, 1981.
-
- M. Verigin (e-mail: verigin@iki.rssi.ru), G. Kotova, A. Szabo, J. Slavin, T. Gombosi, K. Kabin, F. Shugaev, and A. Kalinchenko